UDC 546.26:539.89

Z. S. Zhao (Qinhuangdao, Hebei, China)
X.-F. Zhou (Tianjin, China)
M. Hu, D. L. Yu, J. He (Qinhuangdao, Hebei, China)
H.-T. Wang (Tianjin, China)
Y. J. Tian, B. Xu (Qinhuangdao, Hebei , China)

High-pressure behaviors of carbon nanotubes

In this paper, we have reviewed the experimental and theoretical studies on pressure-induced polygonization, ovalization, racetrack–shape deformation, and polymerization of carbon nanotubes (CNTs). The corresponding electronic, optical, and mechanical changes accompanying these behaviors have been discussed. The transformations of armchair (n, n) CNT bundles (n = 2, 3, 4, 6, and 8) under hydrostatic or nonhydrostatic pressure into new carbons, including recently proposed superhard bct-C_4, Cco-C_8, and B-B_1A_{L2R2} carbon phases have also been demonstrated. Given the diversity of CNTs from various chiralities, diameters, and arrangements, pressure-induced CNT polymerization provides a promising approach to produce numerous novel metastable carbons exhibiting unique electronic, optical, and mechanical characteristics.

Keywords*: pressure-induced carbon nanotubes, polymerization, novel metastable carbons, electronic and mechanical characteristics.*

INTRODUCTION

Carbon adopts a wide range of allotropes with unique physical and chemical properties, e.g., graphite, diamond, fullerenes, nanotubes, chaoite, graphene, and amorphous carbon due to its ability to form *sp*-, sp^2-, and sp^3-hybridized bonds. Graphite, the most stable form of carbon at ambient pressure, has a layered and planar structure with the stacked graphene layers coupled by delocalized weak π bonds resulting in conductive and soft nature. Graphene, a recently rising star material, is one-atom-thick planar sheet with a honeycomb crystal lattice like that of graphite. Graphene has the amazing conductivity and strongest tensile strength along the planar layer directions but flexile in the other directions because of the conductive, strong, and flexile sp^2 bonds.

Fullerenes and carbon nanotubes (CNTs) represent another two classes of fully sp^2 bonding carbons and are the focus of modern nanoscience and nanotechnology. Structurally, fullerenes are hollow graphitic cage structures composed of nonplanar 5- and 6-membered carbon rings. The smallest fullerene is C_{20} [1]. Larger fullerene with increased diameter can also be formed [2, 3]. Among them, purified C_{60} and C_{70} are now commercially available. CNTs can be considered as seamless cylinders formed by rolling single- or multilayer graphene. Different rolling manners yield distinct diametral and chiral CNTs. Given these unique configurations, CNTs possess a wide range of chemical and physical properties, e.g., low density, versatile electronic properties (insulating, semiconducting, or conducting states), and excellent mechanical performance (approximately 1 TPa of axial Young's modulus and approximately 150 GPa of axial tensile strength) [4].

Thus, CNTs are ideal materials for applications as chemical catalysts/absorbents, in nanoscale electronic devices, and in the mechanical engineering industry. However, anisotropic CNTs are extraordinarily flexible in their radial direction and are prone to deformation or collapse under external forces.

Pressure is an effective means to induce the sp^2-to-sp^3 bond change in carbon, and the produced metastable carbon phases strongly depend on the crystal structure and hybridization scheme of raw carbons, as well as on applied hydrostatic/nonhydrostatic pressure. For example, the compression of graphite can experimentally yield cubic and hexagonal diamonds, as well as a superhard cold-compressed post-graphite phase [5–10]. The glass carbon under pressure can transform into a superhard amorphous diamond [11], whereas the compression of C_{60} and C_{70} fullerenes can produce interesting 1D, 2D, and 3D C_{60} and C_{70} polymers, as well as other elusive new carbon phases [12–25]. Because a variety of CNT configurations can now be synthesized with a high yield, more interesting pressure-induced structural, electronic, and mechanical changes in CNTs are expected and have elicited considerable attention [26–29].

In this paper, we review experimental and theoretical progress of the behaviors of CNTs under pressure. Solid evidence has indicated that polygonization, ovalization, racetrack-shape deformation, and polymerization of CNTs depend on the diameter, chirality, and stacking style of single- or multi-walled CNTs under hydrostatic and nonhydrostatic pressures. When the applied pressure is sufficiently high, one-dimensional (1D) CNTs would polymerize or collapse to form 3D-linked CNTs or other metastable carbon species, which are promising candidates for superhard and superstrong structural materials.

EXPERIMENTAL

In the initial experiments under low pressure, the structural changes in single-walled CNT (SWCNTs) bundles were revealed via Raman and X-ray diffraction (XRD) resonances. In aligned SWCNTs Raman investigation showed that the intensity of radial breathing modes (around 180 cm^{-1}) decreased significantly with respect to that of the tangential modes (G bands around 1590 cm^{-1}) with increased pressure [30]. The disappearance of the radial breathing modes were confirmed at 1.5 [26], 1.7 [31], 2.6 [30], or 3 [32] GPa by different research groups. This disappearance can be attributed to the loss of electronic resonance in the Raman scattering cross-section due to the deformation of circular nanotubes into a hexagonal or oval configuration under compression. However, Merlen et al. [33] discovered that the critical pressure for the disappearance of radial breathing modes depends on the wavelength of the laser used for Raman measurement. The study further indicated that this may not be an effective indicator for structural transition [33]. The tangential mode frequencies of aligned SWCNTs show an interesting variation trend with increasing pressure, characterized by an initial increase until 11 GPa, then a decrease until 16 GPa, and an increase again beyond 16 GPa [30, 32]. This anomalous pressure dependence was also attributed to the hexagonal and elliptical cross-section of deformed tubes [30, 32]. Notably, the intensity and frequency of the Raman modes of SWCNTs in the aforementioned experiments are reversible upon decompression. Moreover, high-pressure XRD experiments reveal the loss of the triangular lattice above 1.5 GPa in SWCNT bundles [34]. The triangular lattice can be regenerated upon decompression if the pressure is lower than 4 GPa, beyond which the nanotube lattice is destroyed [34]. In contrast, another experiment discovered the critical pressure for the reversible lattice of

SWCNT bundles increases up to 13 GPa, indicating the remarkable mechanical resilience of CNTs [35].

The structural changes in CNTs result in corresponding electronic and optical modifications. With applied pressure, non-monotonic variation was observed in the resistance of SWCNT bundles at room temperature and up to 2 GPa [36]. In addition, local metallization spatially confined to a few nanometers was identified by radial compression at a crossed junction of semiconducting CNTs [37]. The optical absorption spectra of SWCNTs were observed to change drastically and reversibly at pressures up to 4.1 GPa [38], with a structural phase transition occurring at approximately 2 GPa [39].

The influence of nonhydrostatic high pressure is more promising for deformed CNTs to produce new carbon phases. X-ray Raman scattering (XRS) experiments were performed with multi-walled CNTs (MWCNTs) under nonhydrostatic pressure up to 25 GPa [19]. Variation in near-edge peaks represented decreased sp^2 hybridization and increased sp^3 hybridization in compressed MWCNTs with increasing pressure. At 16 GPa, the spectral features completely resembled the spectrum of diamonds with no sp^2 contribution, indicating the formation of a hard, sp^3 hybridized carbon phase. This argument was further supported by the optical transparency of the samples, i.e., the compressed MWCNTs were black and opaque at 0.3 GPa and became partially transparent at 11 GPa.

Another study of the compression of SWCNTs demonstrated that a quenchable superhard carbon phase could be obtained at a nonhydrostatic pressure of 24 GPa [40, 41]. The nonhydrostatic effect was achieved by shear deformation under load in a diamond anvil cell. The final product exhibited a high bulk modulus (465 GPa) and hardness (62 to 150 GPa) comparable to those of diamond. The transformation was accompanied by irreversible changes in Raman spectra. The Raman band frequencies in the new carbon phase are consistent with those in the raw SWCNTs, with broadening of *G* bands at approximately 1551 to 1598 cm^{-1} and an increased intensity of the *D* band at approximately 1344 cm^{-1}. The polymerization of CNTs was concluded based on the conservation of the spectral features of CNTs in Raman spectra of treated carbon samples.

Another quenchable superhard carbon phase was obtained by compressing SWCNTs under a nonhydrostatic pressure of 35 GPa [42]. When the nonhydrostatic effect was achieved by applying shear deformation at 35 GPa (leading to a pressure multiplication up to 60 GPa), the intensity and width of the Raman *G* bands of compressed SWCNTs abruptly increased without frequency change, which is similar to the features observed in the aforementioned carbon obtained at a nonhydrostatic pressure of 24 GPa [40, 41]. The carbon product possesses a mixture of sp^2 and sp^3 hybridizations with approximately 40% sp^2 states. The maximum photoluminescence band was about 2 eV corresponding to an optical gap of 2.1 to 2.3 eV. The hardness was 58±6 GPa, comparable to that of cubic boron nitride. Transmission electron microscopy (TEM) analysis of this superhard phase revealed nanoclusters with turbostratic, curved graphene sheets. Another quenchable superhard crystalline carbon allotrope was recovered from CNT bundles compressed at 75 GPa and room temperature [43]. This allotrope has high density (3.6±0.2 g/cm^3) and high bulk modulus (447 GPa). More importantly, this carbon allotrope can crack diamond and thus, has elicited considerable research interest [44–47].

Other interesting nano- and microcrystalline diamond-like (cubic and hexagonal) and nanographite carbon phases have been synthesized by SWCNT treatments at pressures ranging from 8.0 to 9.5 GPa and temperatures ranging from

473 to 1773 K [48]. Using shock compression of approximately 120 GPa at 2000 K, most MWCNTs was transformed into graphite structures with increased spacing between graphene planes [49]. Although significant experimental progress has been achieved by compressing CNTs, the crystal structures of most of these new carbons cannot be determined from experimental observations alone. Thus, theoretical endeavors are highly anticipated to eliminate structural uncertainty and controversy.

THEORETICAL SECTION

This section firstly discusses results of pressure-induced structural, electronic, and mechanical changes for isolated SWCNTs. Previous studies showed that the isolated armchair (*n*, *n*) and zigzag (*n*, 0) SWCNTs exhibit metallic and semiconducting properties at ambient pressure, respectively [50, 51]. During compression, isolated armchair (8, 8) and (10, 10) SWCNTs underwent a series of changes from circular, to oval, to racetrack-like, and, finally, to peanut-like shapes, resulting in a metal-to-semiconductor transition (Fig. 1) [52, 53]. The isolated zigzag (10, 0), (13, 0), and (19, 0) SWCNTs also showed similar shape changes under hydrostatic pressure [54]. The smallest (10, 0) CNTs deformed continuously, whereas larger (13, 0) and (19, 0) CNTs exhibited hysteresis and underwent a first-order-like transformation [54]. Pressure-induced hard-to-soft transition based on decreased bulk modulus was observed in isolated SWCNTs with different diameters ranging from armchair (5, 5) to (20, 20) CNTs because of the circular-to-oval shape transition of the tubes at low pressure [55]. However, nanoindentation simulation demonstrated that isolated CNTs underwent a soft-to-hard phase transformation under compressive stresses higher than 16 GPa because of the formation of interlayer sp^3 bonds [56]. This transformation was reversible upon unloading if the compressive stress was under approximately 70 GPa, beyond which the permanent interlayer sp^3 bonds formed [56]. During nanoindentation, the maximum nanohardness of CNTs can reach 120 GPa, which is comparable to that of diamond [56].

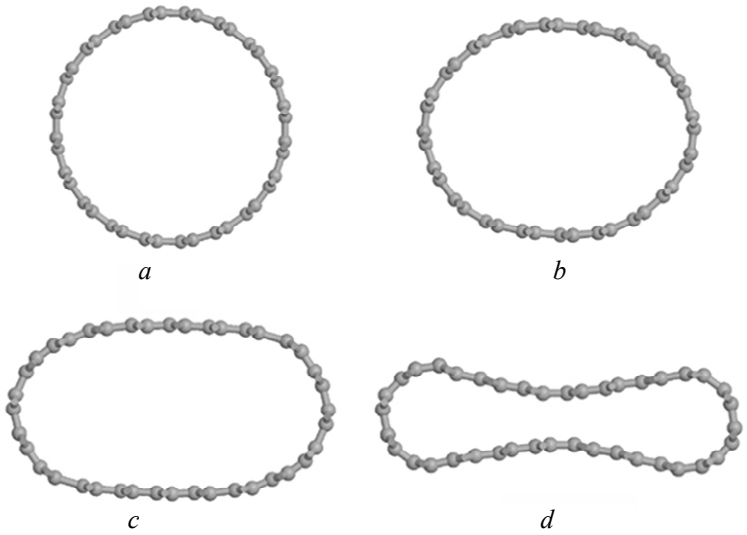

Fig. 1. Molecular-dynamics simulated equilibrium shapes of an isolated (10, 10) SWCNT at pressures of (*a*) 0, (*b*) 1.55, (*c*) 1.75, and (*d*) 2.2 GPa, respectively [53].

In the case of bundled CNTs, the intertube interaction would greatly affect the behaviors of CNTs at ambient pressure. For small zigzag (n, 0) SWCNT bundles with high curvature energy, (5, 0) and (6, 0) CNTs can be spontaneously enthalpy-driven and directly cross-linked to create 2D CNTs at ambient pressure (Fig. 2, *a*) [57]. Another theoretical study also confirmed the preferable thermodynamic stability of 2D-linked (5, 0) and (6, 0) CNTs at ambient pressure compared with corresponding van der Waals-packed CNTs [58]. For (n, 0) SWCNTs, a linked 2D structure prevails at ambient pressure for $n < 7$, whereas individual nanotube bundle structures are adapted for $n > 7$ [57]. In contrast to zigzag (n, 0) SWCNTs, the cross-linking of small armchair (n, n) SWCNTs, such as (3, 3) and (4, 4) CNTs, was not spontaneous at ambient pressure [57]. This may be due to adjacent armchair tubes in bundle aligned "shoulder-by-shoulder" with local structures similar to that in flattened graphene sheets, whereas in the zigzag tubes they are virtually aligned "head-to-head" and are thus prone to bond formation [57].

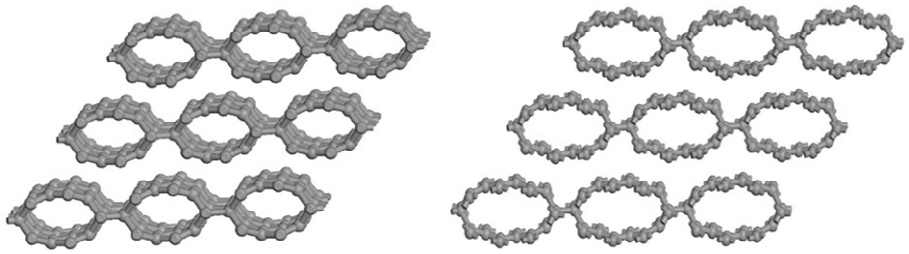

a *b*

Fig. 2. (*a*) 2D cross-linked (5, 0) CNTs at ambient pressure [57] and (*b*) 2D cross-linked (7, 0) CNTs at 0.3 GPa [58].

At ambient pressure the cross-section of aligned CNTs in bundles is not always circular. Hexagonal, oval, and racetrack-like shapes are predominantly driven by intertube wall-to-wall interaction. Research has suggested that (6n, 6n) SWCNTs such as (6, 6) and (12, 12) CNTs have hexagonal cross-sections in bundles at ambient pressure [59]. This is in reasonable agreement with the experimental study of the polygonization of aligned tubes with a diameter of approximately 17 Å corresponding to (12, 12) nanotubes, where rounded-hexagonal cross-sections in bundles were observed without applied pressure [60]. For other SWCNT bundles, such as (8, 8), (10, 10), (24, 0), and (30, 0), oval-shaped cross sections were observed at ambient pressure [59]. In addition, unlike the metallic isolated armchair SWCNTs, an opening of the band gap resulting from weak intertube interactions and slight nanotube deformation was observed in armchair (4, 4), (5, 5), (6, 6), (7, 7), (9, 9), (10, 10), and (12, 12) SWCNT bundles at ambient pressure [61].

When pressure was added, all aligned CNTs underwent structural transitions with the cross-section changing from circular, to oval or hexagonal, or racetrack-like [29, 62, 63], and, finally, to 2D- or 3D-linked CNTs or complicated carbon phases [58, 61, 64, 65]. The transition or collapse pressure varied with the symmetry, chirality, and diameter of the CNTs [29, 59, 64, 66–69]. Usually, the larger the diameters of CNT bundles are, the lower the transition pressure will be [29, 59, 64, 66–69]. Sluiter et al. [64] predicted a complete SWCNT phase diagram under pressure that depended mainly on the tube diameter. Researchers have observed that (3n + 3, 3n + 3) SWCNT bundles such as (12, 12) and (9, 9) acquire

a hexagonal cross-section when subjected to hydrostatic pressures of 6 GPa and 10 GPa, respectively [61, 62]. Other single-walled (8, 8), (10, 10), (24, 0), and (30, 0) CNT bundles exhibited an oval cross-section at low pressure [59]. In addition, many 2D- and 3D-linked CNTs emerged at high pressure and remained stable after pressure release. The lowest transition pressure from (7, 0) CNTs to 2D-linked (7, 0) CNTs was 0.3 GPa (Fig. 2, *b*) [58], far lower than the 10 GPa obtained in another research [61]. The 2D interlinked (5, 5) and (12, 12) CNTs were formed under respective hydrostatic pressures of 18 and 8 GPa [61].

Previous studies showed that 1D (6, 6) CNTs did not form an interlinked structure even at 60 GPa because of the repulsive interaction between the local flattened adjacent layers during compression [58]. Our study shows this equilibrium state will be broken and 3D-linked deformed (6, 6). CNTs can be formed at pressures as high as 80 GPa (Fig. 3). This situation is similar to the formation of 3D-linked (3, 3) CNTs [70], where the lowest pressure needed to overcome the repulsion of the π bonds in local flattened layers to form σ bonds was 40 GPa. More complicated stable 3D structures can be produced by compressing various CNTs including (5, 0), (7, 0), (9, 0), (6, 6), (7, 7), (10, 10), (7, 4), mixed (6, 6) and (7, 7), and mixed (6, 6) and (7, 4) SWCNTs, as well as double-walled CNTs such as (5, 5), (10, 10), and composite of C_{60} and CNTs (Fig. 4) [58, 65, 71]. They form a large family of carbons where either full sp^3 hybridization or mixed sp^2 and sp^3 hybridizations are presented. Some of them exhibit high thermodynamic stability and excellent mechanical performance (e.g., bulk modulus) comparable to cubic diamond.

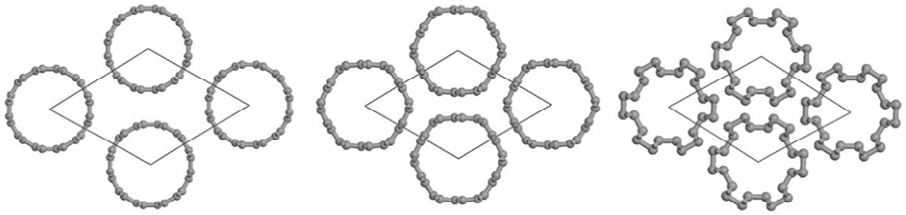

a *b* *c*

Fig. 3. The aligned 1D (6, 6) CNTs at (*a*) ambient pressure and (*b*) 60 GPa [58], and (*c*) 3D-linked (6, 6) CNTs at 80 GPa in present work.

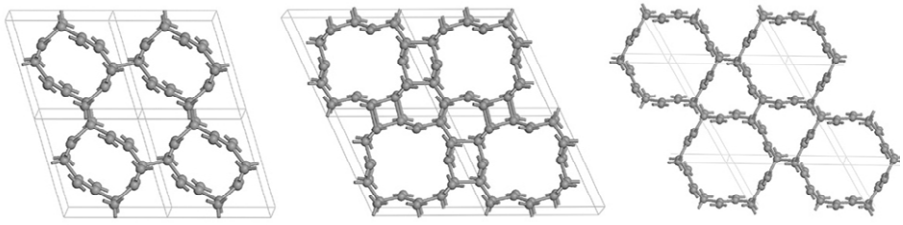

a *b* *c*

Fig. 4. The 3D-linked (*a*) (5, 0), (*b*) (7, 0), and (*c*) (9, 0) CNTs configurations obtained by compressing corresponding CNTs [58].

Recently, numerous theoretical simulations have been performed to identify experimentally synthesized and structurally unknown superhard, cold-compressed

CNTs [43] and graphite [5–9]. We first proposed Cco-C_8, a sp^3-bonded carbon structure, which can be viewed as 3D-linked (2, 2) CNTs to satisfactorily account for the density, X-ray diffraction data, bulk modulus, and hardness of the experimentally observed superhard cold-compressed CNTs [46]. Later, Niu et al. [47] suggested alternative carbon models including *P*-carbon and B-B_1A_{L2R2}-carbon. The proposed M–carbon is the first model to successfully explain the experimental XRD, optical transparency, and superhard nature of cold-compressed graphite [72, 73]. After that, a series of models including bct-C_4 [74, 75]; *W*-carbon [76]; structurally equivalent Cco-C_8 [46], Z-carbon [77], oC16-II [78], and Z-carbon-8 [79]; structurally equivalent F-carbon [80], S-carbon [47], Z-carbon-1 [79], and M10-carbon [81]; structurally equivalent O-carbon [82], R-carbon [47], and H-carbon [83, 84]; structurally equivalent Z4-A3B1 [85] and P-carbon[47]; structurally equivalent S-carbon [83, 84] and C-carbon [86]; X-carbon and Y-carbon [87] were proposed. Recently, the high-pressure experiments and transition path sampling calculations indicate M-carbon is the most likely product of cold compression of graphite [88–91]. These studies offer in-depth understanding of the behaviors of CNTs and graphite under pressure. Moreover, the chiral C_6 [92], and cubic C_3 [93], *Cmcm*-16 [94], *Cmcm*-12 [94], *P*2/*m*-8 [94] and three charming superhard carbons, i.e., hP3, tI12, and tP12, with significantly greater density than diamond [95] were also proposed.

Experimental evidence has been found for the existence of the smallest zigzag (4, 0), armchair (2, 2), and (3, 3) SWCNTs confined inside larger nanotubes [96–98]. We thus explore the transformations of single-walled armchair (*n*, *n*) CNT bundles (*n* = 2, 3, 4, 6, 8) under hydrostatic or nonhydrostatic pressures, resulting in new carbons including the proposed bct-C_4 [74, 75], Cco-C_8 [46], B-B_1A_{L2R2}-carbon [47], 3D-linked (3, 3) CNTs [70, 99], 3D-linked (6, 6) CNTs, and 3D-linked (8, 8) CNTs (Figs. 5–8). Under hydrostatic pressure of 5 GPa, a (2, 2) CNT bundle with hexagonal and tetragonal lattices would polymerize to form 3D-linked (2, 2) CNTs, i.e., Cco-C_8 and bct-C_4 (Fig. 5). In contrast, nonhydrostatic pressure is needed to form bct-C_4, Cco-C_8, and B-B_1A_{L2R2}-carbon by compressing larger (*n*, *n*)

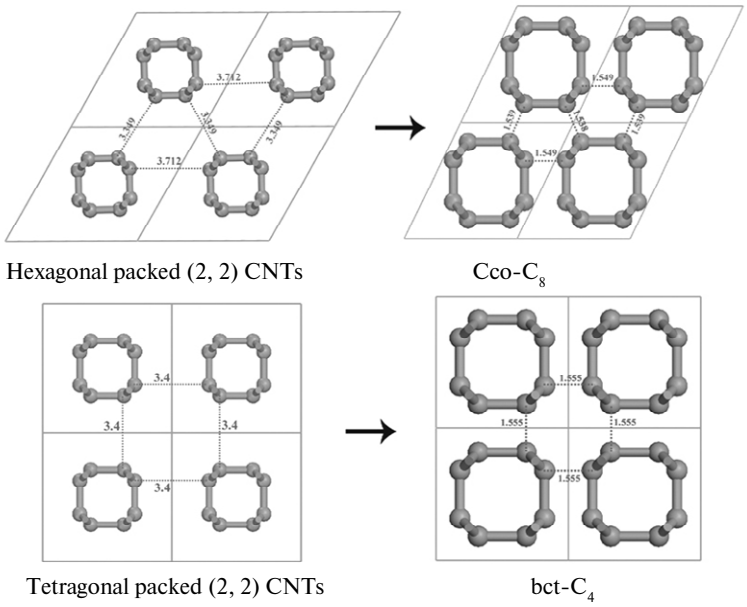

Fig. 5. Cco-C_8 and bct-C_4 carbons obtained by compressing hexagonal and tetragonal packed (2, 2) CNTs at 5 GPa, respectively.

CNTs. For example, a (4, 4) CNT bundle under pressure first forms 3D-linked (4, 4) CNTs [99] through 2 + 2 cycloaddition, similar to the formation of the well-known 3D C_{60} polymers [14]. This is then flattened to form bct-C_4 or Cco–C_8 carbons (Fig. 6). During compression, larger (6, 6) and (8, 8) CNT bundles are first flattened and polymerized to form 3D-linked CNTs and finally B-B_1A_{L2R2}-carbon or Cco-C_8 (Fig. 7). Under hydrostatic pressures of 80 and 50 GPa, two 3D-linked (6, 6) CNTs can be formed by compressing hexagonal and tetragonal (6, 6) CNT bundles, respectively (Figs. 3 and 8). All the structural data of these considered 3D-linked CNTs are listed in Table 1. Our studies show, by compressing armchair (*n*, *n*) CNTs bundles, new carbon species with 4- and 8-membered carbon rings, which are different from the common 6-membered rings of diamond, can easily be formed. Other novel metastable carbons are expectedly obtained by compressing various single- and multi-walled CNTs with different chiralities and manners of stacking.

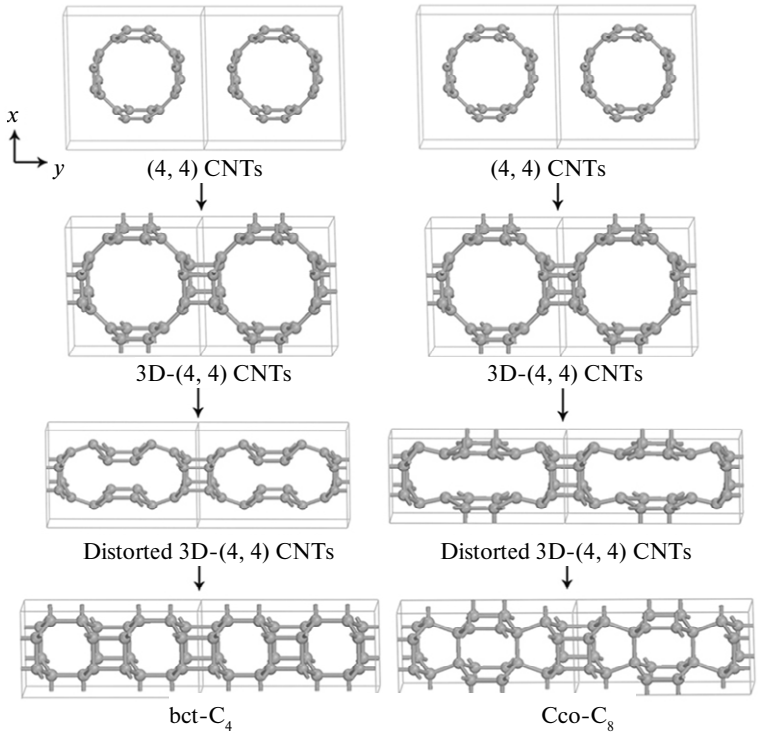

Fig. 6. Cco-C_8 and bct-C_4 carbons obtained by compressing identical tetragonal packed (4, 4) CNTs at nonhydrostatic pressure (y = 38 GPa, $x = z$ = 40 GPa). At this pressure, the occurrence frequency of Cco-C_8 is higher than that of bct-C_4.

The experimental bulk and shear modulus of CNT bundles are reported to be 41.7 GPa and 1 GPa, respectively [34, 100], similar to those of soft graphite, due to comparable weak van der Waals interactions. The most striking properties of 3D CNT polymers are their very high hardness and strength, both of which can now be estimated by using our semi-empirical formula [101–105]. The hardness formulas for semiconducting and metallic carbons are $H_V = 350N_e^{2/3}e^{-1.191f_i}/d^{2.5}$ and $H_V = 350N_e^{2/3}e^{-1.191f_i - 32.2f_m^{0.55}}/d^{2.5}$, respectively. N_e is the valence electron density, valued as $N_e = n_cZ_c/V$, whereas n_c is the number of C atoms in the unit cell,

Z_c is the valence electron number of C atoms which is equal to 4, and V is the volume of a unit cell; f_i is the Phillips ionicity of the C−C bond, which is equal to 0; f_m is a factor of metallicity, calculated using $f_m = 0.026D_F/n_e$, with D_F being the total density of states of a unit cell at the Fermi level, and n_e the total number of valence electrons in the unit cell; d is the average C−C bond length, calculated using $d = \sum_j N^j d^j \Big/ \sum_j N^j$, with N^j being the number of the j bond in the unit cell, and d^j, the j bond length.

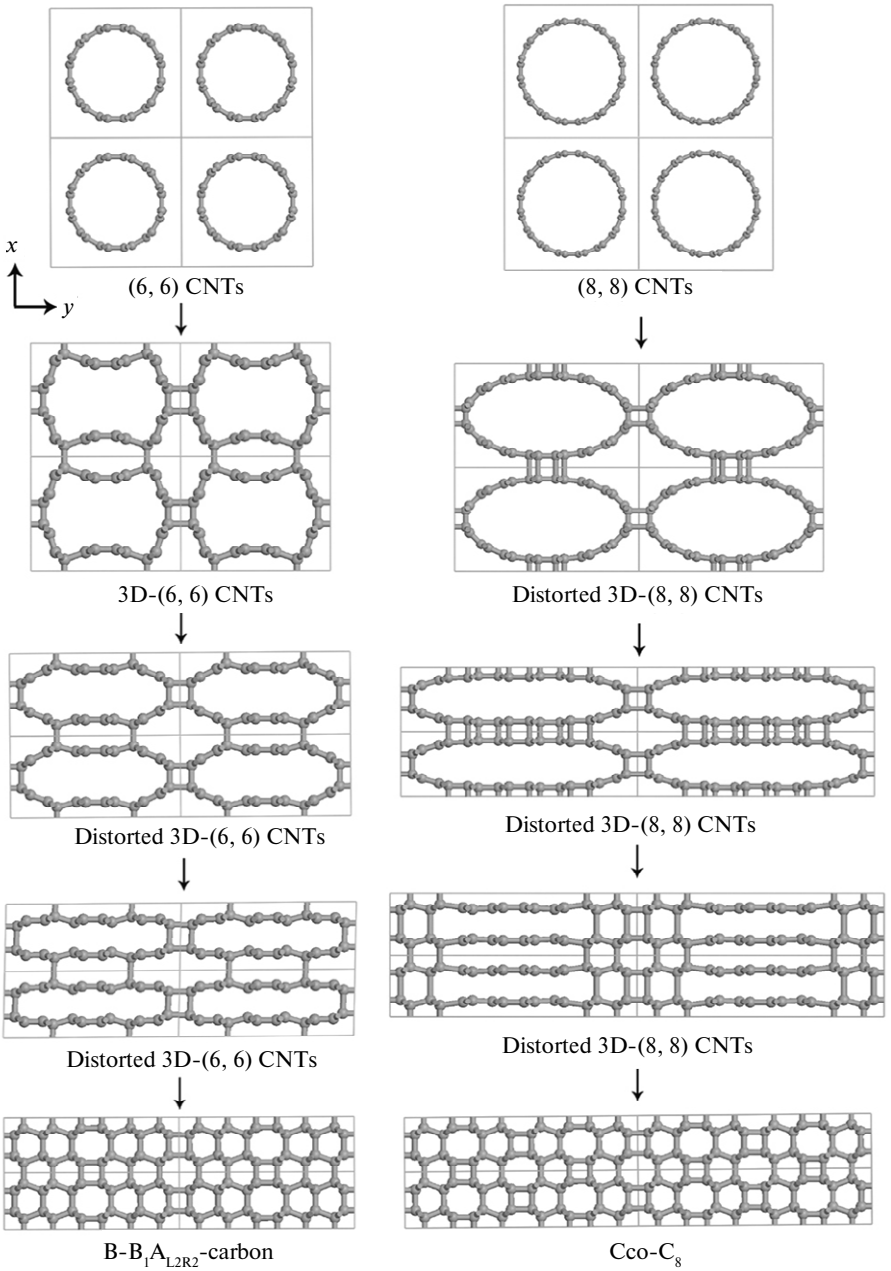

Fig. 7. B-B_1A_{L2R2}-carbon and Cco-C_8 carbon obtained by compressing tetragonal packed (6, 6) and (8, 8) CNTs at nonhydrostatic pressure (y = 36 GPa, $x = z$ = 40 GPa) and (y = 40 GPa, $x = z$ = 60 GPa), respectively.

Table 1. The space group, lattice parameters (Å), and atomic positions of 3D-linked SWCNTs at ambient pressure

Structures	Space group	*a*	*b*	*c*	β	Atomic positions
3D-(5, 0)	*Cmcm* (63)	7.368	9.778	4.172		16*h* (0.720, –0.060, 0.085)
						16*h* (0.679, 0.198, 0.066)
						8*f* (0.5, 0.230, 0.588)
3D-(7, 0)	*P*21/*m* (11)	6.966	4.193	7.259	113.50	4*f* (0.888, 0.065, 0.928)
						4*f* (0.849, 0.590, 0.731)
						4*f* (0.902, 0.071, 0.582)
						4*f* (0.856, 0.571, 0.375)
						4*f* (0.693, 0.066, 0.188)
						4*f* (0.488, 0.588, 0.159)
						4*f* (0.290, 0.064, 0.016)
3D-(9, 0)	*P*63/*mcm* (193)	9.296		4.200		24*l* (–0.148, 0.275, 0.586)
						12*k* (0, 0.418, 0.433)
Bct-C_4 [74]	*I*4/*mmm* (139)	4.322		2.478		8*h* (0.18, 0.18, 0)
Cco-C_8 [46]	*Cmmm* (65)	8.674	4.209	2.487		8*q* (–1/6, –0.815, –1/2)
						8*p* (–0.089, –0.315, 0)
3D (3, 3)-I [70]	*R*-3*m* (166)	10.394		2.467		36*i* (0.048, 0.244, 1.262)
3D-(3, 3)-II [99]	*Cmmm* (65)	6.071	2.482	5.201		4*k* (1/2, –1.5, –0.128)
						4*h* (0.319, –1, –1/2)
						4*l* (1/2, –1, –0.718)
3D-(4, 4) [99]	*P*4/*mmm* (123)	5.173		2.480		4*n* (1/2, 0.717, 0)
						4*o* (0.129, 1/2, 1/2)
3D-(6, 6)-I	*P*6/*mmm* (191)	8.961		2.488		12*p* (1.498, 1.335, 0)
						12*q* (1.385, 1.287, 0.5)
3D-(6, 6)-II	*P*42/*mmc* (131)	8.568		2.445		8*q* (0.842, 0.583, 0)
						8*q* (0.833, 0.907, 0)
						8*q* (0.860, 0.662, 0.5)
3D-(8, 8)	*P*4/*mmm*(123)	9.742		2.484		8*q* (0.775, 0.650, 1/2)
						8*q* (0.912, 0.728, 1/2)
						8*p* (0.922, 0.815, 1)
						8*p* (0.763, 0.568, 1)
B-B_1A_{L2R2} [47]	*Immm* (71)	4.179	12.968	2.484		8*n* (0.815, 0.560, 0)
						8*n* (0.687, 0.778, 0)
						8*n* (0.685, 0.611, 0.5)

In our tensile strength calculation model [99, 105], the theoretical tensile strength in a specified [*hkl*] direction is microscopically determined by the bond strength and broken bond number (bond density) in the corresponding (*hkl*) crystal plane. Usually, the (*hkl*) plane with the least broken bond number (i.e., the lowest bond density) is selected, whereas the lowest bond density in the (*hkl*) plane usually determines the ideal tensile strength. The bond strength of the *i*–*j* bond is proposed to be equal to the maximum tensile force F_{ij} of the unbinding *i*–*j* bond and proven exclusively dependent on two microscopic parameters: bond length d_{ij}

and effectively bonded valence electron (EBVE) number n_{ij}. Here n_{ij} can be calculated from the expression: $n_{ij} = n_i n_j \Big/ \sqrt{n_i^2 + n_j^2}$ with $n_j = Z_i/N_j$ and $n_i = Z_i/N_i$, where Z_i and Z_j are the valence electron numbers of atom i and j, respectively (for C, they are both equal to 4); and N_i and N_j are the coordination numbers of atoms i and j, respectively. F_{ij} is calculated using $F_{ij}(N) = 6.6 \cdot 10^{-10} d_{ij}^{-1.32} \exp(3.7 n_{ij})$. Finally, the theoretical tensile strength σ_{hkl} along the [*hkl*] direction can be calculated using $\sigma_{hkl}^{theor}(\text{Pa}) = F_{ij} S_{hkl}$, where S_{hkl} (m^{-2}), is the number of the broken bonds per unit area in the (*hkl*) plane with the lowest bond density.

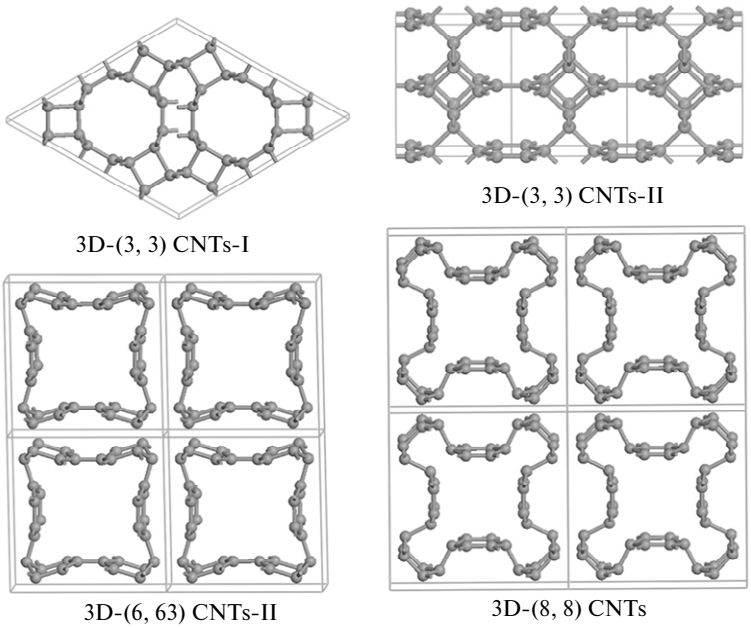

Fig. 8. 3D-(3, 3) CNT-I, 3D-(6, 6) CNT-II, and 3D-(8, 8) CNTs obtained at 40, 50, and 60 GPa, respectively. The previously proposed 3D-(3, 3) CNT-II [99] is also shown.

The hardness and strength models have been widely applied to covalence-dominant crystals, such as the light-element B–C–N–O system [46, 74, 80, 95, 99, 106–117] and transition-metal B–C–N–O compounds [102, 104, 118–124], and other high hardness materials [125–127]. Table 2 lists the calculated bandgap, density, Young's moduli, tensile strength, bulk modulus, shear modulus, and Vickers hardness of some 3D-linked SWCNTs composed of small CNTs. Our calculations show that they are all superhard materials, and the metallic carbons have lower hardness. It should be noted that our hardness model may be not suitable for 3D-linked large CNTs with very high pores, where increased sp^2-hybridized bonds can sustain large distortions through out-of-plane bending without breaking under stress. As a comparison, their hardness values can also be estimated by other models such as Simunek's [128], Xue's [129], Chen's [130], Lyakhov's [94], and Mukhanov's models [131]. On the other hand, our strength model can be used to estimate the tensile strength of any direction of all the metastable carbons. All the investigated 3D-linked CNTs have high axial tensile strength comparable to that of CNTs, while exhibiting greatly enhanced strength in the radial direction through sp^3 bond buckling. Compared with 1D CNTs, the 3D-

linked CNTs have the obvious increase of Young's, bulk, and shear moduli, which can also be attributed to the solid sp^3 bonds in structures. In addition to these excellent mechanical properties, these 3D-linked CNTs also have novel electrical properties (e.g., semimetallic, metallic, and semiconducting with a wide range of bandgaps), representing a class of multipurpose carbon materials.

Table 2. The bandgap (eV), density (g·cm^{-3}), axial Young's moduli Y_a (TPa), radial Young's moduli Y_r (TPa), axial tensile strength σ_a (GPa), radial tensile strength σ_r (GPa), bulk moduli B (GPa), shear moduli G (GPa), B/G ratio, and Vickers hardness H_V (GPa) of 3D-linked SWCNTs at ambient pressure

Structure	Bandgap	Density	Y_a	Y_r	σ_a	σ_r	B	G	B/G	H_V
3D-(5, 0)	semimetallic	2.65	0.98	0.22	147.3	27.7	267.4	196.8	1.36	87.6
3D-(7, 0)	1.98	2.87	1.04	0.45	100.0	73.5	280.5	276.0	1.02	81.6
3D-(9, 0)	metallic	2.28	0.91	0.27	134.0	97.2	252.8	176.3	1.43	53.4
Bct-C_4	2.71	3.45	1.23	0.94	112.2	93.2	415.6	434.2	0.96	92.9
							414 [74]	427 [74]		
Cco-C_8	3.14	3.51	1.22	1.15	113.0	93.4	415.6	434.2	0.96	95.1
							444.1 [46]			[46]
3D-(3, 3)-I [70]	2.88	3.1	1.11	0.70	76.5	118.6	347.1	343.5	1.01	85.5
3D-(3, 3)-II [99]	1.21	3.05	1.13	0.49	129.9	76.5	343.9	283.5	1.21	90.9
3D-(4, 4) [99]	0.93	2.40	0.93	0.57	114.1	115.1	277.6	140.4	1.98	79.8
3D-(6, 6)-I	1.26	2.77	0.92	0.34	85.5	33.1	267.2	214.7	1.24	79.9
3D-(6, 6)-II	metallic	2.67	1.11	0.57	178.7	128.6	278.5	207.7	1.34	59.4
3D-(8, 8)	1.92	2.71	0.96	0.45	101.8	59.1	281.9	192.8	1.46	81.7
B-B_1A_{L2R2}	3.18	3.56	1.23	1.15	115.3	94.1	438.9	506.7	0.90	96.2
							456.3 [47]	504.4 [47]		

CONCLUSIONS

In the present paper, the experimental and theoretical researches on high-pressure behaviors of carbon nanotubes have been reviewed. It seems that a deep gap exists in the nice theoretical structures and real substances prepared under pressure. In real experiments some amorphous and nanostructured mash consisted of quite small fragments of initial nanotubes are usually fabricated due to the shear stresses, inhomogeneities, impurities, geometrical structure restrictions, etc. If the CNTs with controllable chirality and diameter can be achieved in the near future, experimental synthesis of the specific theoretical structures may be easy at nice pressure conditions, like the case of the C_{60} polymers recovered from the compression of high spherically symmetric C_{60} fullerenes.

Anyway, it is theoretically demonstrated that CNTs under pressure can be a better candidate for producing novel carbon phases stemming from their diverse fascinating configurations, as determined by chirality, diameter, length, and number of graphene layers. The unique 3D CNT polymers and other complicated metastable carbons derived from CNTs are expected to be classified into a new family of superhard and superstrong structural materials with potential applications in many fields. CNT analogs, such as boron nitride, silicon, and germanium

nanotubes, may have similar high-pressure behaviors as CNTs and elicit corresponding theoretical and experimental explorations. In the end, we wish to emphasize that, in addition to pressure, which can induce the linkage of CNTs, other experimental means (e.g., electron-beam irradiation) can also stimulate linkage in CNT bundles [132, 133], thus providing tremendous impetus for further experimental investigations.

ACKNOWLEDGMENT

This work was supported by NBRPC (Grant No. 2011CB808205), NSFC (Grants No. 51121061, No. 91022029, and No. 11174152), and the Science Foundation of Yanshan University for the Excellent Ph.D. Students (Grant No. YSUSF201101).

Розглянуто експериментальні та теоретичні дослідження з індукованою тиском полігонізації, овалізації, деформації у формі бігової доріжки і полімеризації вуглецевих нанотрубок (ВНТ). Обговорено відповідні електронні, оптичні і механічні зміни, що супроводжують ці процеси. Також продемонстровано перетворення в ВНТ у формі крісла (n, n), зібраних в пучок (n = 2, 3, 4, 6 і 8) під гідростатичним або негідростатичним тиском в нові вуглецеві алотропи, в тому числі недавно запропоновані надтверді bct-C_4, Cco-C_8 і B-B_1A_{L2R2}-вуглецеві фази. Різноманітність ВНТ з різними хіральністю, діаметрами та упаковками, а також полімеризація ВНТ, викликана тиском, забезпечує перспективний підхід для отримання численних нових метастабільних вуглецевих фаз, що демонструють унікальні електронні, оптичні і механічні характеристики.

***Ключові слова**: вуглецеві нанотрубки під тиском, полімеризація, нові метастабільні форми вуглецю, електронні та механічні характеристики.*

Рассмотрены экспериментальные и теоретические исследования по индуцированной давлением полигонизации, овализации, деформации в форме беговой дорожки и полимеризации углеродных нанотрубок (УНТ). Обсуждены соответствующие электронные, оптические и механические изменения, сопровождающие эти процессы. Также продемонстрированы преобразования в УНТ в форме кресла (n, n), собранных в пучок (n = 2, 3, 4, 6 и 8) под гидростатическим или негидростатическим давлением в новые углеродные аллотропы, в том числе недавно предложенные сверхтвердые bct-C_4, Cco-C_8 и B-B_1A_{L2R2}-углеродные фазы. Разнообразие УНТ с различными хиральностью, диаметрами и упаковками, а также полимеризация УНТ, вызванная давлением, обеспечивает перспективный подход для получения многочисленных новых метастабильных углеродных фаз, демонстрирующих уникальные электронные, оптические и механические характеристики.

***Ключевые слова**: углеродные нанотрубки под давлением, полимеризация, новые метастабильные формы углерода, электронные и механические характеристики.*

1. *Prinzbach H., Weiler A., Landenberger P. et al.* Gas-phase production and photoelectron spectroscopy of the smallest fullerene, C_{20} // Nature. – 2000. – **407**, N 6800. – P. 60–63.
2. *Parker D. H., Wurz P., Chatterjee K. et al.* High-Yield synthesis, separation, and mass-spectrometric characterization of fullerenes C_{60} to C_{266} // J. Am. Chem. Soc. – 1991. – **113**, N 20. – P. 7499–7503.
3. *Huang J., Ding F., Jiao K., Yakobson B. I.* Real time microscopy, kinetics, and mechanism of giant fullerene evaporation // Phys. Rev. Lett. – 2007. – **99**, N 17, art. 175503.
4. *Demczyk B., Wang Y., Cumings J. et al.* Direct mechanical measurement of the tensile strength and elastic modulus of multiwalled carbon nanotubes // Mater. Sci. Eng.: A. – 2002. – 334, N 1. – P. 173–178.
5. *Bundy F. P., Kasper J. S.* Hexagonal diamond – a new form of carbon // J. Chem. Physics. – 1967. – **46**, N 9. – P. 3437–3446.
6. *Yagi T., Utsumi W., Yamakata M.-A. et al.* High-pressure *in situ* x-ray-diffraction study of the phase transformation from graphite to hexagonal diamond at room temperature // Phys. Rev. B. – 1992. – **46**, N 10. – P. 6031–6039.

7. *Miller E. D., Nesting D. C., Badding J. V.* Quenchable transparent phase of carbon // Chem. Mater. – 1997. – **9**, N 1. – P. 18–22.
8. Patterson J. R., Kudryavtsev A., Vohra Y. K. X-ray diffraction and nanoindentation studies of nanocrystalline graphite at high pressures // Appl. Phys. Lett. – 2002. – **81**, N 11. – P. 2073–2075.
9. *Mao W. L., Mao H.-K., Eng P. J. et al.* Bonding changes in compressed superhard graphite // Science. – 2003. – **302**, N 5644. – P. 425–427.
10. *Kurio A., Tanaka Y., Sumiya H. et al.* Wear resistance of nano-polycrystalline diamond with various hexagonal diamond contents // J. Superhard Mater. – 2012. – **34**, N 6. – P. 343–349.
11. *Lin Y., Zhang L., Mao H.-K. et al.* Amorphous diamond: a high-pressure superhard carbon allotrope // Phys. Rev. Lett. – 2011. – **107**, N 17, art. 175504.
12. *Iwasa Y., Arima T., Fleming R. M. et al.* New phases of C_{60} synthesized at high pressure // Science. – 1994. – **264**, N 5165. – P. 1570–1572.
13. *Marques L., Hodeau J. L., Núñez-Regueiro M., Perroux M.* Pressure and temperature diagram of polymerized fullerite // Phys. Rev. B. – 1996. – **54**, N 18. – P. R12633–R12636.
14. *Blank V. D., Buga S. G., Dubitsky G. A. et al*. High-pressure polymerized phases of C_{60} // Carbon. – 1998. – **36**, N 4. – P. 319–343.
15. *Okada S., Saito S.* Electronic structure and energetics of pressure-induced two-dimensional C_{60} polymers // Phys. Rev. B. – 1999. – **59**, N 3. – P. 1930–1936.
16. *Patterson J. R., Catledge S. A., Vohra Y. K. et al*. Electrical and mechanical properties of C_{70} fullerene and graphite under high pressures studied using designer diamond anvils // Phys. Rev. Lett. – 2000. – **85**, N 25. – P. 5364–5367.
17. *Ponyatovsky E., Tonkov E. Y.* Phase Transformations of Elements under High Pressure. – London, New York, Washington: CRC Press Boca Raton, 2004. – 392 p.
18. *Yamanaka S., Kubo A., Inumaru K. et al.* Electron conductive three-dimensional polymer of cuboidal C_{60} // Phys. Rev. Lett. – 2006. – **96**, N 7, art. 076602.
19. *Kumar R. S., Pravica M. G., Cornelius A. L. et al.* X-ray Raman scattering studies on C_{60} fullerenes and multi-walled carbon nanotubes under pressure // Diamond Relat. Mater. – 2007. – **16**, N 4–7. – P. 1250–1253.
20. *Sundqvist B.* Fullerenes under high pressures // Adv. Physics. – 1999. – **48**, N 1. – P. 1–134.
21. *Soldatov A. V., Roth G., Dzyabchenko A. et al.* Topochemical polymerization of C_{70} controlled by monomer crystal packing // Science. – 2001. – **293**, N 5530. – P. 680–683.
22. *Makarova T. L., Sundqvist B., Hohne R. et al*. Magnetic carbon // Nature. – 2001. – **413**, N 6857. – P. 716–718.
23. *Brazhkin V. V., Lyapin A. G.* Hard carbon phases prepared from fullerite C_{60} under high pressure // New Diamond Front Carbon Technol. – 2004. – **14**, N 5. – P. 259–278
24. *Sundqvist B.* Polymeric fullerene phases formed under pressure // Structure & Bonding. – 2004. – **109**. – P. 85–126.
25. *Brazhkin V. V., Lyapin A. G.* Hard and superhard carbon phases synthesised from fullerites under pressure // J. Superhard Mater. – 2012. – **34**, N 6. – P. 400–423.
26. *Venkateswaran U. D., Rao A. M., Richter E. et al.* Probing the single-wall carbon nanotube bundle: Raman scattering under high pressure // Phys. Rev. B. – 1999. – **59**, N 16. – P. 10928–10934.
27. *Loa I.* Raman spectroscopy on carbon nanotubes at high pressure // J. Raman Spectroscopy. – 2003. – **34**, N 7–8. – P. 611–627.
28. *Zang J., Treibergs A., Han Y., Liu F.* Geometric constant defining shape transitions of carbon nanotubes under pressure // Phys. Rev. Lett. – 2004. – **92**, N 10, art. 105501.
29. *Gadagkar V., Maiti P. K., Lansac Y. et al.* Collapse of double-walled carbon nanotube bundles under hydrostatic pressure // Phys. Rev. B. – 2006. – **73**, N 8, art. 085402.
30. *Sood A. K., Teresdesai P. V., Muthu D. V. S. et al.* Pressure behaviour of single wall carbon nanotube bundles and fullerenes: a Raman study // Phy. Stat. Sol. (b). – 1999. – **215**, N 1. – P. 393–401.
31. *Peters M. J., McNeil L. E., Lu J. P., Kahn D.* Structural phase transition in carbon nanotube bundles under pressure // Phys. Rev. B. – 2000. – **61**, N 9. – P. 5939–5944.
32. *Teredesai P.V., Sood A.K., Sen R. et al.* Pressure-induced reversible transformation in single-wall carbon nanotube bundles studied by Raman spectroscopy // Chem. Phys. Lett. – 2000. – **319**, N 3–4. – P. 296–302.
33. *Merlen A., Bendiab N., Toulemonde P. et al.* Resonant Raman spectroscopy of single-wall carbon nanotubes under pressure // Phys. Rev. B. – 2005. – **72**, N 3, art. 035409.

34. *Tang J., Qin L.-C., Sasaki T., Yudasaka M. et al.* Compressibility and polygonization of single-walled carbon nanotubes under hydrostatic pressure // Phys. Rev. Lett. – 2000. – **85**, N 9. – P. 1887–1889.
35. *Sharma S. M. Karmakar S. Sikka S. K. et al.* Pressure-induced phase transformation and structural resilience of single-wall carbon nanotube bundles // Phys. Rev. B. – 2001. – **63**, N 20, art. 205417.
36. *Gaál R., Salvetat J. P., Forró L.* Pressure dependence of the resistivity of single-wall carbon nanotube ropes // Ibid. – 2000. – **61**, N 11. – P. 7320–7323.
37. *Vitali L., Burghard M., Wahl P. et al.* Local pressure-induced metallization of a semiconducting carbon nanotube in a crossed junction // Phys. Rev. Lett. – 2006. – **96**, N 8, art. 086804.
38. *Kazaoui S., Minami N., Yamawaki H. et al.* Pressure dependence of the optical absorption spectra of single-walled carbon nanotube films // Phys. Rev. B. – 2000. – **62**, N 3. – P. 1643–1646.
39. *Kuntscher C.A., Thirunavukkuarasu K., Pekker Á. et al.* Pressure-induced phenomena in single-walled carbon nanotubes // Phys. Stat. Sol. (b). – 2007. – **244**, N 11. – P. 3982–3985.
40. *Popov M., Kyotani M., Nemanich R. J., Koga Y.* Superhard phase composed of single-wall carbon nanotubes // Phys. Rev. B. – 2002. – **65**, N 3, art. 033408.
41. *Popov M., Kyotani M., Koga Y.* Superhard phase of single wall carbon nanotube: comparison with fullerite C_{60} and diamond // Diamond Relat. Mater. – 2003. – **12**, N 3–7. – P. 833–839.
42. *Blank V. D., Denisov V. N., Kirichenko A. N. et al*. Nanostructured superhard carbon phase obtained under high pressure with shear deformation from single-wall nanotubes hipco // Physica B: Condens. Matter. – 2006. – **382**, N 1–2. – P. 58–64.
43. *Wang Z., Zhao Y., Tait K. et al.* A Quenchable superhard carbon phase synthesized by cold compression of carbon nanotubes // Proc. Natl. Acad. Sci. U.S.A. – 2004. – **101**, N 38. – P. 13699–13702.
44. *Bucknum M., Castro E.* The carbon allotrope hexagonite and its potential synthesis from cold compression of carbon nanotubes // J. Chem. Theory Comput. – 2006. – **2**, N 3, art. 775–781.
45. *Zhu C., Guo W., Yu T.* An efficient method for evaluating the nanohardness of layer-configured materials by atomistic simulation // Nanotechnology. – 2007. – **18**, N 29, art. 295704.
46. *Zhao Z., Xu B., Zhou X.-F. et al.* Novel superhard carbon: C-centered orthorhombic C_8 // Phys. Rev. Lett. – 2011. – **107**, N 21, art. 215502.
47. *Niu H., Chen X.-Q., Wang S. et al.* Families of superhard crystalline carbon allotropes constructed via cold compression of graphite and nanotubes // Ibid. – 2012. – **108**, N 13, art. 135501.
48. *Khabashesku V. N., Gu Z., Brinson B. et al.* Polymerization of single-wall carbon nanotubes under high pressures and high temperatures // J. Phys. Chem. B. – 200. – **106**, N 43. – P. 11155–11162.
49. *Molodets A., Golyshev A., Zhukov A. et al*. Structural and morphological changes induced by intense shock waves in carbon nanotubes // Nanotechnologies in Russia. – 2008. – **3**, N 11. – P. 697–703.
50. *Odom T. W., Huang J.-L., Kim P., Lieber C. M.* Atomic structure and electronic properties of single-walled carbon nanotubes // Nature. – 1998. – **391**, N 6662. – P. 62–64.
51. *Ouyang M., Huang J.-L., Cheung C. L., Lieber C. M.* Energy gaps in “metallic” single-walled carbon nanotubes // Science. – 2001. – **292**, N 5517. – P. 702–705.
52. *Lu J.-Q., Wu J., Duan W. et al.* Metal-to-semiconductor transition in squashed armchair carbon nanotubes // Phys. Rev. Lett. – 2003. – **90**, N 15, art. 156601.
53. *Wu J., Zang J., Larade B. et al.* Computational design of carbon nanotube electromechanical pressure sensors // Phys. Rev. B. – 2004. – **69**, N 15, art. 153406.
54. *Tangney P., Capaz R. B., Spataru C. D. et al.* Structural transformations of carbon nanotubes under hydrostatic pressure // Nano Lett. – 2005. – **5**, N 11. – P. 2268–2273.
55. *Sun D. Y., Shu D. J., Ji M. et al.* Pressure-induced hard-to-soft transition of a single carbon nanotube // Phys. Rev. B. – 2004. – **70**, N 16, art. 165417.
56. *Guo W., Zhu C. Z., Yu T. X. et al.* Formation of sp^3 bonding in nanoindented carbon nanotubes and graphite // Phys. Rev. Lett. – 2004. – **93**, N 24, art. 245502.
57. *Cheng H., Pez G. P., Cooper A. C.* Spontaneous Cross linking of small-diameter single-walled carbon nanotubes // Nano Lett. – 2003. – **3**, N 5. – P. 585–587.
58. *Yildirim T., Gülseren O., Kılıç Ç., Ciraci S.* Pressure-induced interlinking of carbon nanotubes // Phys. Rev. B. – 2000. – **62**, N 19. – P. 12648–12651.

59. *Zhang X. H., Sun D.Y., Liu Z. F., Gong X. G.* Structure and phase transitions of single-wall carbon nanotube bundles under hydrostatic pressure // Ibid. – 2004. – **70**, N 3, art. 035422.
60. *Lopez M. J., Rubio A., Alonso J. A. et al.* Novel polygonized single-wall carbon nanotube bundles // Phys. Rev. Lett. – 2001. – **86**, N 14. – P. 3056–3059.
61. *Saxena S., Tyson T. A.* Interacting quasi-two-dimensional sheets of interlinked carbon nanotubes: a high-pressure phase of carbon // ACS Nano. – 2010. – **4**, N 6. – P. 3515–3521.
62. *Sluiter M.H.F., Kumar V., Kawazoe Y.* Symmetry-driven phase transformations in single-wall carbon-nanotube bundles under hydrostatic pressure // Phys. Rev. B. – 2002. – **65**, N 16, art. 161402.
63. *Chan S.-P., Yim W.-L., Gong X.G., Liu Z.-F.* Carbon nanotube bundles under high pressure:transformation to low-symmetry structures // Ibid. – 2003. – **68**, N 7, art. 075404.
64. *Sluiter M.H.F., Kawazoe Y.* Phase diagram of single-wall carbon nanotube crystals under hydrostatic pressure // Phys. Rev. B. – 2004. – **69**, N 22, art. 224111.
65. Sakurai M., Saito S. Pressure-induced structural phase transition of small-diameter carbon nanotubes // Physica E: Low-dimens. Syst. Nanostruct. – 2011. – **43**, N 3. – P. 673–676.
66. *Venkateswaran U. D., Masica D. L., Sumanasekera G. U. et al.* Diameter dependent wall deformations during the compression of a carbon nanotube bundle // Phys. Rev. B. – 2003. – **68**, N 24, art. 241406.
67. *Elliott J. A., Sandler J. K. W., Windle A. H. et al.* Collapse of single-wall carbon nanotubes is diameter dependent // Phys. Rev. Lett. – 2004. – **92**, N 9, art. 095501.
68. Ye X., Sun D. Y., Gong X. G. Pressure-induced structural transition of double-walled carbon nanotubes // Phys. Rev. B. – 2005. – **72**, N 3. – P. 035454.
69. *Imtani A. N., Jindal V. K.* Structure of armchair single-wall carbon nanotubes under hydrostatic pressure // Ibid. – 2007. – **76**, N 19. – P. 195447.
70. *Julong H., Zhisheng Z., Yongjun T.* New three-dimensional (3, 3) carbon nanotube polymers // J. Yanshan University. – 2011. – **35**, N 6. – P. 471–475.
71. *Omata Y., Yamagami Y., Tadano K. et al*. Nanotube nanoscience: a molecular-dynamics study // Physica E: Low-dimens. Syst. Nanostruct. – 2005. – **29**, N 3–4. – P. 454–468.
72. *Li Q., Ma Y., Oganov A. R. et al.* Superhard monoclinic polymorph of carbon // Phys. Rev. Lett. – 2009. – **102**, N 17, art. 175506.
73. *Oganov A. R., Glass C. W.* Crystal structure prediction using ab initio evolutionary techniques: principles and applications // J. Chem. Phys. – 2006. – **124**, N 24, art. 244704.
74. *Zhou X. F., Qian G. R., Dong X. et al. Ab initio* study of the formation of transparent carbon under pressure // Phys. Rev. B. – 2010. – **82**, N 13, art. 134126.
75. *Umemoto K., Wentzcovitch R. M., Saito S., Miyake T.* Body-centered tetragonal C_4: a viable sp^3 carbon allotrope // Phys. Rev. Lett. – 2010. – **104**, N 12, art. 125504.
76. *Wang J.-T., Chen C., Kawazoe Y.* Low-temperature phase transformation from graphite to sp^3 orthorhombic carbon // Ibid. – 2011. – **106**, N 7, art. 075501.
77. *Amsler M., Flores-Livas J. A. Lehtovaara L. et al.* Crystal structure of cold compressed graphite // Ibid. – 2012. – **108**, N 6, art. 065501.
78. *Selli D., Baburin I. A., Martoňák R., Leoni S.* Superhard sp^3 carbon allotropes with odd and even ring topologies // Phys. Rev. B. – 2011. – **84**, N 16, art. 161411.
79. Zhou R., Zeng X. C. Polymorphic phases of sp^3-hybridized carbon under cold compression // J. Am. Chem. Soc. – 2012. – **134**, N 17. – P. 7530–7538.
80. *Tian F., Dong X., Zhao Z. et al.* Superhard F-carbon predicted by *ab initio* particle-swarm optimization methodology // J. Phys.: Condens. Matter. – 2012. – **24**, N 16, art. 165504.
81. *Amsler M., Flores-Livas J. A., Botti S. et al.* Prediction of a novel monoclinic carbon allotrope // Condensed Matter. – 2012. – arXiv:1202.6030v1 [cond-mat.mtrl-sci].
82. *Wang J.-T., Chen C., Kawazoe Y.* Orthorhombic carbon allotrope of compressed graphite: ab initio calculations // Phys. Rev. B. – 2012. – **85**, N 3, art. 033410.
83. *He C., Sun L., Zhang C. et al.* New superhard carbon phases between graphite and diamond // Solid State Comm. – 2012. – **152**, N 16. – P. 1560–1563.
84. *He C. Y., Sun L. Z., Zhong J. X.* Prediction of superhard carbon allotropes from a segment combination method // J. Superhard Mater. – 2012. – **34**, N 6. – P. 386–399.
85. *He C., Sun L., Zhang C. et al.* Four superhard carbon allotropes: a first-principles study // Phys. Chem. Chem. Phys. – 2012. – **14**, N 23. – P. 8410–8414.
86. *Li D., Bao K., Tian F. et al.* Lowest enthalpy polymorph of cold-compressed graphite phase // Ibid. – 2012. – **14**, N 13. – P. 4347–4350.
87. *Zhu Q., Zeng Q., Oganov A. R.* Systematic search for low-enthalpy sp^3 carbon allotropes using evolutionary metadynamics // Phys. Rev. B. – 2012. – **85**, N 20, art. 201407.

88. *Boulfelfel S. E., Oganov A. R., Leoni S.* Understanding the nature of "superhard graphite" // Sci. Rep. – 2012. – **2**. – P. 471.
89. *Wang Y. J., Lee K.K.M.* From soft to superhard: fifty years of experiments on cold-compressed graphite // J. Superhard Mater. – 2012. – **4**, N 6. – P. 360–371.
90. *Wang Y. J., Panzik J. E., Kiefer B., Lee K. K. M.* Crystal structure of graphite under room-temperature compression and decompression // Sci. Rep. – 2012. – **2**, art. 520.
91. *Boulfelfel S. E., Zhu Q., Oganov A. R.* Novel sp^3-forms of carbon predicted by evolutionary metadynamics and analysis of their synthesizability using transition path sampling // J. Superhard Mater. – 2012. – **34**, N 6. – P. 350–359.
92. *Pickard C. J., Needs R.* Hypothetical low-energy chiral framework structure of group 14 elements // Phys. Rev. B. – 2010. – **81**, N 1, art. 014106.
93. *Wang J. T., Chen C., Kawazoe Y.* New cubic carbon phase via graphitic sheet rumpling // Ibid. – 2012. – **85**, N 21, art. 214104.
94. *Lyakhov A. O., Oganov A. R.* Evolutionary search for superhard materials: methodology and applications to forms of carbon and TiO_2 // Ibid. – 2011. – **84**, N 9, art. 092103.
95. *Zhu Q., Oganov A. R., Salvadó et al.* Denser than diamond: ab initio search for superdense carbon allotropes // Ibid. – 2011. – **83**, N 19, art. 193410.
96. *Qin L.-C., Zhao X., Hirahara K. et al.* Materials science: the smallest carbon nanotube // Nature. – 2000. – **408**, N 6808, art. 50.
97. *Zhao X., Liu Y., Inoue S. et al.* Smallest carbon nanotube is 3 Å in diameter // Phys. Rev. Lett. – 2004. – **92**, N 12, art. 125502.
98. *Peng L. M., Zhang Z. L., Xue Z. Q. et al.* Stability of carbon nanotubes: how small can they be? // Ibid. – 2000. – **85**, N 15. – P. 3249–3252.
99. *Zhao Z., Xu B., Wang L.-M. et al.* Three dimensional carbon-nanotube polymers // ACS Nano. – 2011. – **5**, N 9. – P. 7226–7234.
100. *Salvetat J.-P., Briggs G. A. D., Bonard J.-M. et al.* Elastic and shear moduli of single-walled carbon nanotube ropes // Phys. Rev. Lett. – 1999. – **82**, N 5. – P. 944–947.
101. *Gao F., He J., Wu E. et al.* Hardness of covalent crystals // Ibid. – 2003. – **91**, N 1. – P. 015502.
102. *Guo X., Li L., Liu Z. et al.* Hardness of covalent compounds: roles of metallic component and *d* valence electrons // J. Appl. Phys. – 2008. – **104**, N 2, art. 023503.
103. *He J., Wu E., Wang H. et al.* Ionicities of boron-boron bonds in B_{12} icosahedra // Phys. Rev. Lett. – 2005. – **94**, N 1. – P. 015504.
104. *Tian Y., Xu B., Zhao Z.* Microscopic theory of hardness and design of novel superhard crystals // Int. J. Refract. Met. Hard Mater. – 2012. – **33**. – P. 93–106.
105. Guo X., Wang L.-M. Xu, B. et al. Unbinding force of chemical bonds and tensile strength in strong crystals // J. Phys.: Condens. Matter. – 2009. – **21**, N 48, art. 485405.
106. *Zhou X. F., Sun J., Fan Y. X. et al*. Most likely phase of superhard BC_2N by *ab initio* calculations // Phys. Rev. B. – 2007. – **76**, N 10, art. 100101.
107. *Liu Z., He J., Yang J. et al.* Prediction of a sandwichlike conducting superhard boron carbide: first-principles calculations // Ibid. – 2006. – **73**, N 17, art. 172101.
108. *He J., Guo L., Guo X. et al.* Predicting hardness of dense C_3N_4 polymorphs // Appl. Phys. Lett. – 2006. – **88**, N 10, art. 101906.
109. *Sun J., Zhou X. F., Qian G. R. et al.* Chalcopyrite polymorph for superhard BC_2N // Ibid. – 2006. – **89**, N 15, art. 151911.
110. *Guo X., Liu Z., Luo X. et al.* Theoretical hardness of the cubic BC_2N // Diamond Relat. Mater. – 2007. – **16**, N 3. – P. 526–530.
111. *Guo X., He J., Liu Z. et al.* Bond ionicities and hardness of $B_{13}C_2$-like structured by X crystals (X = C, N, O, P, As) // Phys. Rev. B. – 2006. – **73**, N 10, art. 104115.
112. Luo X., Guo X., Liu Z. et al. First-principles study of wurtzite BC_2N // Ibid. – 2007. – **76**, N 9. – P. 092107.
113. *Luo X., Zhou X. F., Liu Z. et al.* Refined crystal structure and mechanical properties of superhard BC_4N crystal: first-principles calculations // J. Phys. Chem. C. – 2008. – **112**, N 25. – P. 9516–9519.
114. *Xu L., Zhao Z., Wang L. M. et al.* Prediction of a three-dimensional conductive superhard material: diamond-like BC_2 // Ibid. – 2010. – **114**, N 51. – P. 22688–22690.
115. Liu, H., Li, Q., Zhu, L. and Ma, Y., Superhard and superconductive polymorphs of diamond-like BC_3 // Phys. Lett. A. – 2011. – **375**, N 3. – P. 771–774.
116. *Li Q., Wang H., Tian Y. et al.* Superhard and superconducting structures of BC_5 // J. Appl. Phys. – 2010. – **108**, N 2, art. 023507.

117. *Li Y., Li Q., Ma Y.* B_2CO: a potential superhard material in the BCO system // EPL (Europhysics Letters). – 2011. – **95**, N 6, art. 66006.
118. *Zhao Z., Wang M., Cui L. et al.* Semiconducting superhard ruthenium monocarbide // J. Phys. Chem. C. – 2010. – **114**, N 21. – P. 9961–9964.
119. *Zhao Z., Xu L., Wang M. et al.* Prediction of a conducting hard ductile cubic IrC // Phys. Stat. Sol. (RRL)-Rap. Res. Lett. – 2010. – **4**, N 8–9. – P. 230–232.
120. *Zhao Z., Xu L., Wang L. M. et al.* Superconducting ultraincompressible hard cubic Re_4C // Comput. Mater. Sci. – 2011. – **50**, N 5. – P. 1592–1596.
121. *Sangiovanni D., Hultman L., Chirita V.* Supertoughening in B1 transition metal nitride alloys by increased valence electron concentration // Acta Mater. – 2011. – **59**, N 5. – P. 2121–2134.
122. *Wang Q., Zhao Z., Xu L. et al.* Novel high-pressure phase of RhB: first-principles calculations // J. Phys. Chem. C. – 2011. – **115**, N 40. – P. 19910–19915.
123. *Guo X., Xu B., He J. et al.* Structure and mechanical properties of osmium carbide: first-principles calculations // Appl. Phys. Lett. – 2008. – **93**, N art. 041904.
124. *Zhao Z., Cui L., Wang L. M. et al.* Bulk Re_2C: crystal structure, hardness, and ultraincompressibility // Crystal Growth & Design. – 2010. – **10**, N 12. – P. 5024–5026.
125. *He J., Guo L., Yu D. et al.* Hardness of cubic spinel Si_3N_4 // Appl. Phys. Lett. – 2004. – **85**, N 23. – P. 5571–5573.
126. *Zhang X., Chen Z., Du H. et al.* Potential superhard cubic spinel CSi_2N_4: first-principles investigations // J. Appl. Phys. – 2008. – **103**, N 8, art. 083533.
127. *Wang H., Li Q., Liu H. et al.* Design of superhard ternary compounds under high pressure: SiC_2N_4 and Si_2CN_4 // J. Phys. Chem. C. – 2010. – **114**, N 18. – P. 8609–8613.
128. *Šimůnek A., Vackář J.* Hardness of covalent and ionic crystals: first-principle calculations // Phys. Rev. Lett. – 2006. – **96**, N 8, art. 085501.
129. *Li K., Wang X., Zhang F., Xue D.* Electronegativity identification of novel superhard materials // Ibid. – 2008. – **100**, N 23, art. 235504.
130 *Chen X.-Q., Niu H., Li D., Li Y.* Modeling hardness of polycrystalline materials and bulk metallic glasses // Intermetallics. – 2011. – **9**, N 9. – P. 1275–1281.
131. *Mukhanov V. A., Kurakevych O. O., Solozhenko V. L.* Thermodynamic aspects of materials' hardness: prediction of novel superhard high-pressure phases // High Press. Res. – 2008. – **28**, N 4. – P. 531–537.
132. *Kis A., Csanyi G., Salvetat J. P. et al.* Reinforcement of single-walled carbon nanotube bundles by intertube bridging // Nat. Mater. – 2004. – **3**, N 3. – P. 153–157.
133. *Banhart F.* Structural transformations in carbon nanoparticles induced by electron irradiation // Phys. Solid State. – 2002. – **44**, N 3. – P. 399–404.

State Key Laboratory of Metastable Materials Science
and Technology, Yanshan University
School of Physics and MOE Key Laboratory
of Weak-Light Nonlinear Photonics, Nankai University

Received 21.09.2012